The current issue and full text archive of this journal is available at
www.emeraldinsight.com/0961-5539.htm

Role of experiments in the accurate numerical simulation of thermal processes

Yogesh Jaluria
Department of Mechanical and Aerospace Engineering, Rutgers University, Piscataway, New Jersey, USA

Received 23 November 2009
Revised 21 January 2010
Accepted 2 February 2010

Abstract

Purpose – Experimental results play a crucial role in the validation of mathematical and numerical models for a variety of basic and applied thermal transport problems. The purpose of this paper is to focus on the role played by experimentation in an accurate numerical simulation of thermal processes and systems.

Design/methodology/approach – The paper takes the form of a numerical simulation combined with experimentation. The paper presents various circumstances where the numerical simulation may be efficiently combined with experimentation, and indeed driven by experimental data, to obtain accurate, valid and realistic numerical predictions.

Findings – The paper demonstrates validation and accuracy of numerical simulation.

Originality/value – This paper is an important first step in combining experiments and simulation for complex thermal systems.

Keywords Simulation, Experimentation, Accuracy, Heat transfer, Numerical analysis

Paper type Research paper

1. Introduction

Numerical simulation of fundamental and practical problems, that involve convective heat transfer, is widely used to understand the underlying phenomena and to design, control and optimize thermal systems. Simulation involves mathematical modelling, which gives rise to the governing equations and the relevant boundary conditions, numerical modelling, which results in the discretized form of these equations, and the implementation of the model on a computer to obtain numerical results at a finite number of locations. Numerical modelling and simulation are extensively used because of the limited applicability of analytical methods, particularly for practical applications, which are generally quite complicated, and the expense and time involved in experimental methods (Jaluria, 2008). However, the model is usually validated by the use of analytical and experimental results, if available. Experimental results are also valuable for physical insight and basic understanding. However, besides validation and physical insight, experiments are needed in a wide range of problems to initiate and proceed with the numerical simulation, to obtain greater convenience, accuracy or efficiency in the solution, or to provide necessary inputs for accurate results. This paper focuses on circumstances where the simulation is strongly dependent or driven by the experimental data.

Of particular interest in this review paper are the following aspects:

- material characteristics and properties;

The author acknowledges the support of the National Science Foundation, through several grants, for much of the work reported here. The support from Corning, Inc., for donated fibre coating equipment and optical fibre, is also acknowledged. The author also acknowledges the interactions with Professors D. Knight, T. Rossmann and C. Polymeropoulos, and the work done by several students, as referenced here, that made it possible to present this review.

International Journal of Numerical Methods for Heat & Fluid Flow
Vol. 20 No. 5, 2010
pp. 467-491
© Emerald Group Publishing Limited
0961-5539
DOI 10.1108/09615531011048204

- validation;
- experimentally obtained boundary conditions;
- solution of inverse problems with experimental inputs; and
- concurrent simulation and experimentation.

All these aspects are important for accurate, efficient and convenient numerical simulation of practical convection heat transfer problems. The basic considerations involved in each are presented in this paper, along with examples from areas such as materials processing and cooling of electronic equipment to illustrate the approaches. Experimentation is needed to provide the material properties needed for the simulation, as well as data for validation of the mathematical and numerical models. In many problems, experimental results are needed to quantify the boundary conditions. In some cases, experiments can be obtained only over a limited region or domain and an inverse problem has to be solved to obtain the relevant conditions. Finally, there are circumstances where experimentation is more convenient, accurate and efficient than numerical simulation, whereas the latter may be more appropriate in other circumstances. Then, a combination of experimentation and numerical simulation can be used concurrently to solve the problem most efficiently and accurately. All these aspects are considered in detail in this paper.

Figure 1 shows some common convective heat transfer problems in which numerical simulation has been used to provide the inputs for design and for understanding the basic processes involved. The systems are shown include heat rejection from the condensers of a power plant to a water body such as a lake, an electronic system consisting of three isolated heat sources, representing electronic devices, in an enclosure with forced flow driven by a fan, a horizontal chemical vapour

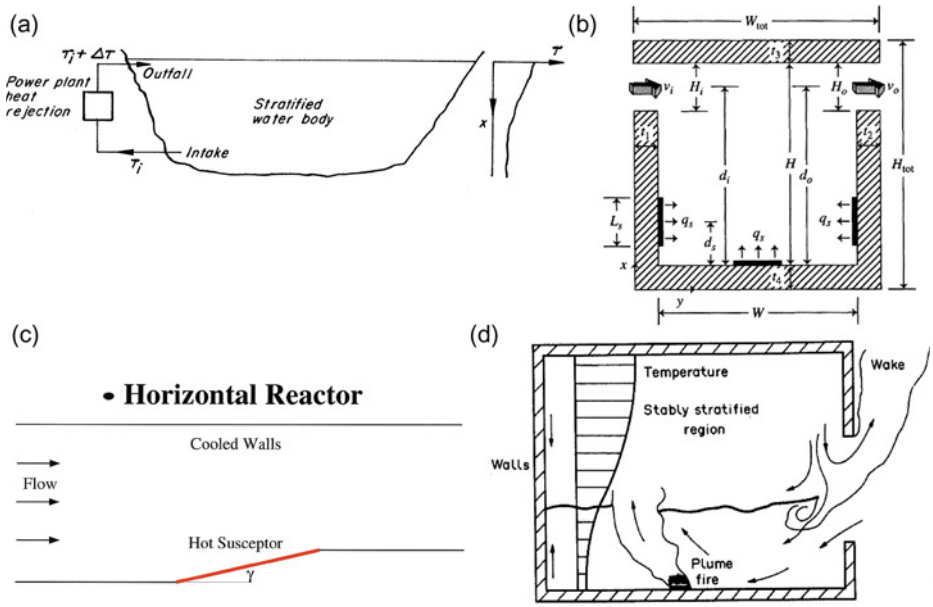

Figure 1.
Examples of practical convective heat transfer problems

Notes: (a) Heat rejection from a power plant; (b) cooling of an electronic system; (c) CVD reactor; and (d) fire in an enclosed region

deposition (CVD) reactor in which chemical reactions result in the deposition of a thin film on the hot susceptor, and a room with a fire showing the stratified hot upper layer generated in the room due to the fire plume and flow exchange through an opening. Because of complexities such as turbulent flow, combined heat and mass transfer, chemical reactions, complicated geometry, variable material properties, buoyancy effects and combined transport mechanisms, numerical simulation is needed to model the flow and the heat transfer in such thermal processes and systems.

2. Mathematical and numerical modelling

Mathematical modelling is one of the most critical elements in the characterization, control, design and optimization of thermal systems. Practical processes and systems are generally very complicated and must be simplified through idealizations and approximations to make the problem solvable. Once the mathematical model is obtained, resulting in the governing equations and boundary conditions, numerical modelling and simulation are used to obtain results that can be used to characterize the process and provide inputs for design and optimization.

As an example, consider the schematic diagram in Figure 2, which shows the system for the polymer coating of an optical fibre after it is drawn in a furnace. The fibre is coated with a jacketing material for protection against abrasion, to reduce stress induced microbending losses, and for increased strength. Generally, curable acrylates, are used and the wet coating is cured by ultra-violet radiation as it passes through the curing station after the coating applicator. The basic coating process involves drawing the fibre through a reservoir of coating fluid from where it is passed through a die that may be used to control the thickness and the concentricity of the coating layer. Viscous

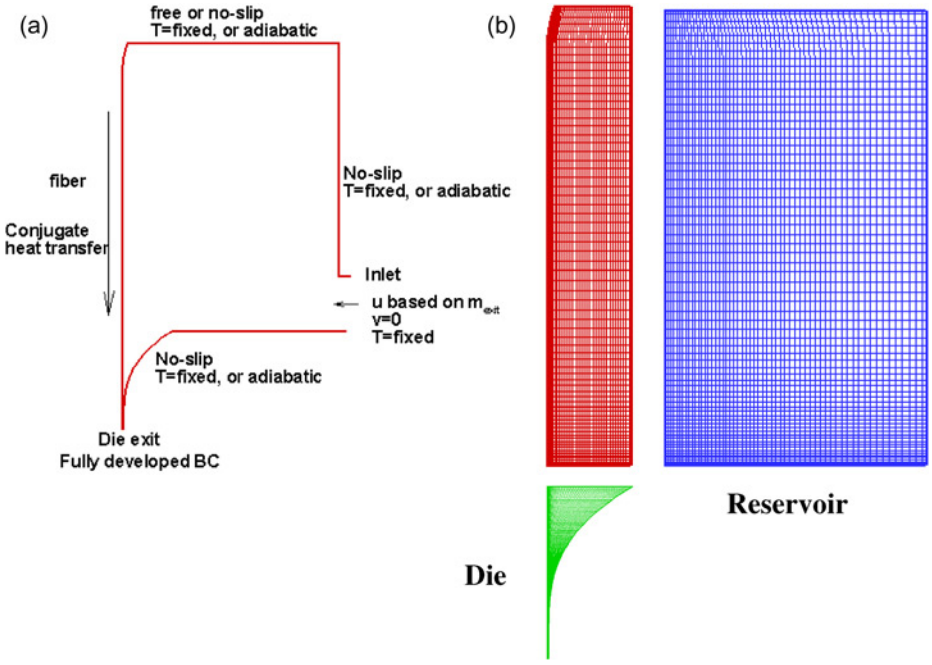

Notes: (a) Optical fibre coating system and (b) grid for numerical simulation

Figure 2.

shear due to the moving fibre results in a circulatory fluid motion within the fluid. A balance between surface tension, viscous, gravitational and pressure forces results in an upstream meniscus at the cup entrance. Similarly, an exit meniscus arises at the bottom of the applicator. This process is considered in some detail later.

If the boundary conditions are well defined, as shown in Figure 2(a), the flow and heat transfer in the coating applicator and the die can be investigated numerically. The governing equations are:

Continuity equation:

$$\frac{1}{r}\frac{\partial}{\partial r}(\rho v r) + \frac{\partial(\rho v)}{\partial z} = 0. \tag{1}$$

Momentum equation in r-direction:

$$\frac{\partial \rho u}{\partial t} + \frac{1}{r}\frac{\partial}{\partial r}\left(r\rho u^2\right) + \frac{\partial}{\partial z}(\rho v u) = -\frac{\partial p}{\partial r} + \frac{1}{r}\frac{\partial}{\partial r}\left(\mu r \frac{\partial u}{\partial r}\right) + \frac{\partial}{\partial z}\left(\mu \frac{\partial u}{\partial z}\right). + \frac{1}{r}\frac{\partial}{\partial r}\left(\mu r \frac{\partial u}{\partial r}\right) + \frac{\partial}{\partial z}\left(\mu \frac{\partial v}{\partial r}\right) - 2\mu \frac{u}{r^2} + \rho g r. \tag{2}$$

Momentum equation in z-direction:

$$\frac{\partial \rho v}{\partial t} + \frac{1}{r}\frac{\partial}{\partial r}(r\rho u v) + \frac{\partial}{\partial z}\left(\rho v^2\right) = -\frac{\partial p}{\partial z} + \frac{1}{r}\frac{\partial}{\partial r}\left(\mu r \frac{\partial v}{\partial r}\right) + \frac{\partial}{\partial z}\left(\mu \frac{\partial v}{\partial z}\right) + \frac{1}{r}\frac{\partial}{\partial r}\left(\mu r \frac{\partial u}{\partial r}\right) + \frac{\partial}{\partial z}\left(\mu \frac{\partial v}{\partial z}\right) + \rho g z. \tag{3}$$

Energy equation:

$$\frac{1}{r}\frac{\partial}{\partial r}(r\rho c_p u T) + \frac{\partial}{\partial z}(\rho c_p v T) = \frac{1}{r}\frac{\partial}{\partial r}\left(Rr\frac{\partial T}{\partial r}\right) + \frac{\partial}{\partial z}\left(R\frac{\partial T}{\partial z}\right) + q''' + \mu\phi$$
$$\phi = 2\left[\left(\frac{\partial u}{\partial r}\right)^2 + \left(\frac{u}{r}\right)^2 + \left(\frac{\partial v}{\partial z}\right)^2\right] + \left(\frac{\partial u}{\partial z} + \frac{\partial v}{\partial r}\right)^2. \tag{4}$$

A wide variety of numerical methods, such as the SIMPLER algorithm developed by Patankar (1980), are available for the solution of these equations. Figure 2(b) shows the discretization of the computational domain. Three distinct regions are indicated. The first one is close to the fibre, which is around 125 μm in diameter, the second is a larger far-field region approximating the reservoir, where an external pressure and inflow may be imposed, and the third one approximates the exit die. A free surface is assumed at the top and no-slip conditions are employed elsewhere. Clearly, the problem may be solved to obtain the temperature and flow fields, from which the coating layer thickness, stability and uniformity may be studied.

Similarly, in the case of a single-screw extruder, as shown in Figure 3, the problem is complicated by the rotating screw and the complex geometry of the channel. Then, the coordinate system may be fixed to the rotating screw and the channel approximated as a wide channel, so that a two-dimensional flow may be assumed. The channels are

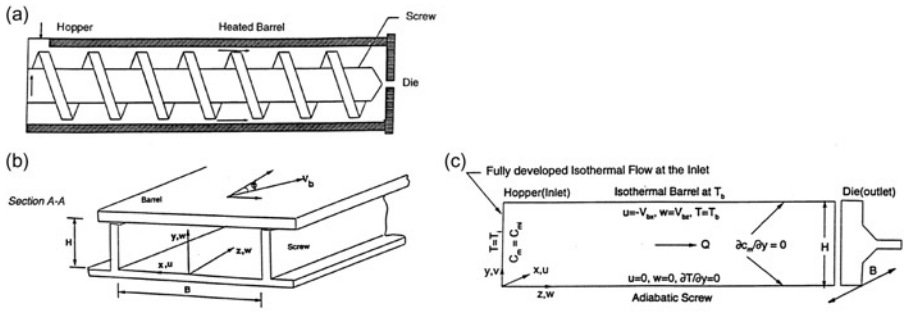

Notes: (a) Schematic of the system; (b) mathematical modelling; and (c) resulting channel flow and coordinate system

Figure 3.
Single-screw polymer extruder

straightened out mathematically, ignoring the effects of curvature. Then the complicated flow in the extruder is replaced by a pressure- and shear-driven channel flow, with shear arising due to the barrel moving at the pitch angle over a stationary screw. This is similar to the shear- and pressure-driven channel flow available in the literature. Therefore, this approximation substantially simplifies the mathematical/numerical model and has been used extensively to obtain the velocity, temperature and pressure distributions in the extruder, from which the torque needed, pressure at the die inlet, and other engineering quantities of interest in the process can be determined (Karwe and Jaluria, 1990; Jaluria, 1996).

3. Material characteristics and properties

Material properties are crucial to the accuracy of any numerical simulation. However, accurate property data are often not available and one has to base the simulation on the information available. Frequently, these data are available at conditions that may be different from those for the actual process, and thus severely limit the usefulness of the simulation. For instance, the manufacture of optical fibres employs the heating of a specially fabricated silica glass preform in a cylindrical furnace above its softening point T_{melt} of around 1,900 K and pulling it into a fibre through a neck-down region (Paek, 1999). The neck-down profile depends strongly upon the drawing conditions, as well as on the physical properties of silica glass, which are strong functions of the temperature T. They also vary with the composition, the main effect being on the radiation properties. The variation in the viscosity is the most critical one for the flow, since it varies quite dramatically with temperature. An equation based on the curve fit of available data for kinematic viscosity ν is written for silica, in SI units, as:

$$\nu = 4,545.45 \exp\left[32\left(\frac{T_{melt}}{T} - 1\right)\right], \tag{5}$$

indicating the strong, exponential, variation of ν with temperature. The radiative source term q''' in the energy equation is non-zero for the glass preform/fibre because glass emits and absorbs energy. The variation of the absorption coefficient with wavelength λ has been measured for certain compositions and glasses, as shown in Figure 4(a). However, such data are often at room temperature, whereas the process itself is at much higher temperatures. Also, data may not be available for the particular glass or composition that is being simulated. Still, such data are extremely valuable and are used

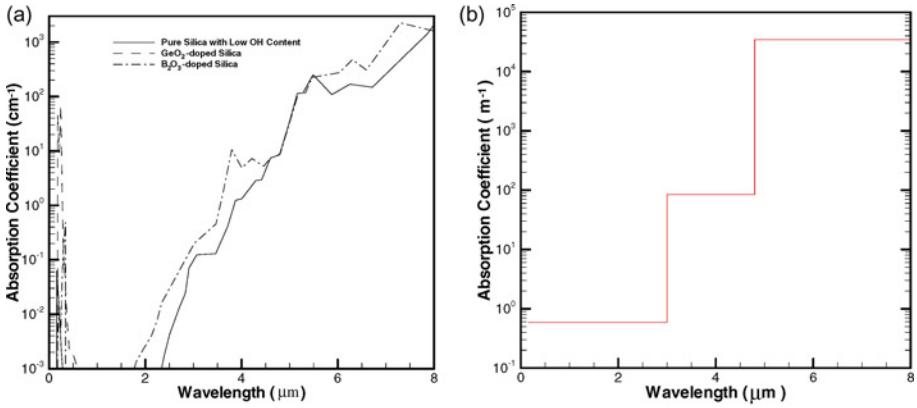

Figure 4.

Notes: (a) Measured absorption coefficient for silica glass and (b) three-band model based on experimental data

in the simulation, often approximating the continuous variation as bands with constant absorption over each band. A two- or three-band absorption coefficient distribution can be effectively used, as shown in Figure 4(b). Then, methods such as the zonal model and the discrete ordinates method can be successfully used to model the radiative transport (Yin and Jaluria, 1997). Other more accurate methods have also been used, though the major constraint has been the availability of accurate radiative property data.

Similarly, the transport processes in polymer processing or coating involve large material property changes. Since the properties may vary with temperature and species concentration, the flow is coupled with the heat and mass transfer problem. However, most materials are also non-Newtonian and the viscosity varies with the shear rate and thus with the flow, making the problem even more complicated. The fluid viscosity is often taken as:

$$\mu = \mu_o(\dot{\gamma}/\dot{\gamma}_o)^{n-1} \exp(b/T), \tag{6}$$

where $\dot{\gamma}$ is the total strain rate, b the temperature coefficient of viscosity, subscript o indicates reference conditions and n is the power-law index of the fluid. The extruded material is thus treated as a Generalized Newtonian fluid (Tadmor and Gogos, 1979). For food materials, the rheological model becomes even more involved because of the dependence on the moisture concentration C. The changes in the chemical structure can also be included as a factor in these equations if experimental data are available. Other constitutive relations for viscosity can easily be employed instead, depending on the material.

4. Validation

An extremely important consideration in the modelling and simulation of thermal processes and systems is that of validation because of the simplifications used to treat various complexities. It is necessary to ensure that the numerical code performs satisfactorily and that the model is an accurate representation of the physical problem. Unless the models are satisfactorily validated and the accuracy of the numerical predictions established, the simulation cannot form the basis for design and optimization. A consideration of the physical behaviour of the results obtained is used

to ensure that the results and trends are physically reasonable. Comparisons with available analytical and numerical results, particularly benchmark solutions, can then be used for validation of the mathematical and numerical models, see, for instance, Roache (1998), de Vahl Davis and Leonardi (2001). Comparisons with experimental results are obviously desirable. Experimental data may be available in some cases and, in others data may be available on similar, though simpler, systems. These may be used for comparisons with numerical results. However, experimental data are often not available and it may become necessary to develop an experimental arrangement for providing inputs for validation. Though this is not a trivial exercise, it could be crucial to establish the validity of the models used, particularly for complex systems on which no other reliable information is available.

Figure 5 shows the comparisons between numerical results and experimental data on a natural lake, such as the one used for heat rejection in Figure 1(a). A one-dimensional model is used, with approximations on mixing due to buoyancy (Moore and Jaluria, 1972). The comparisons are shown for the yearly temperature cycle of the lake, indicating stable stratification in the summer and fully mixed conditions in the winter. Comparisons are also shown for the predicted and measured temperature profiles in the lake. It is interesting to note that, despite substantial complexities in the transport phenomena in the natural lake and the simplicity of the model, the numerical and experimental results show fairly good agreement. This is quite typical for a variety of practical processes, where the overall features are not very sensitive to the model. However, the local velocity and temperature fluctuations and distributions may be quite sensitive and could be used to select the most accurate model.

Similarly, experiments have been carried to validate models for twin-screw extrusion, particularly the transport in the intermeshing region between the two rotating screws. Since the basic phenomena are not very well understood, an experimental system consisting of rotating cylinders was developed and the characteristics of the flow and the basic features of the mixing process in the intermeshing, or mixing, region were investigated (Sastrohartono *et al.*, 1990) (see Figure 6). Experimentally and numerically obtained streamlines in the region between two rotating cylinders, approximating a twin-screw, are shown, indicating good agreement. Some of the fluid flowing adjacent to the left cylinder continues to flow along its surface, while the remaining fluid flows over to the other cylinder. A flow division ratio x_f, defined as the fraction of the mass flow that crosses over from one channel to the other, is taken as a measure of mixing and is determined by using the dividing streamline that separates the two fluid streams. A comparison between

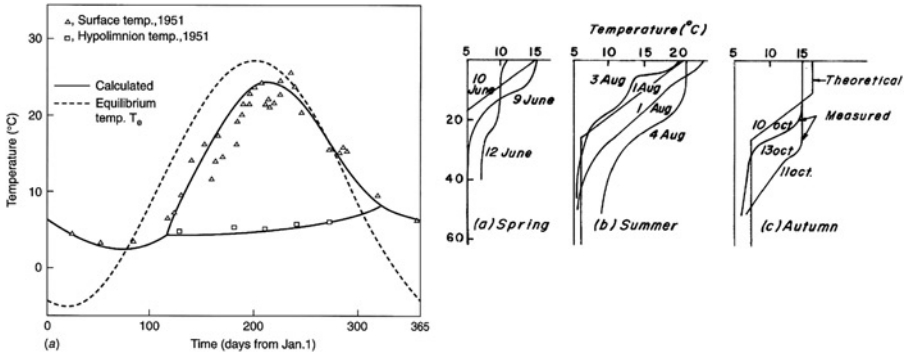

Figure 5.
Predicted yearly temperature cycle of a natural lake and calculated temperature profiles at various times during the year, along with experimental data

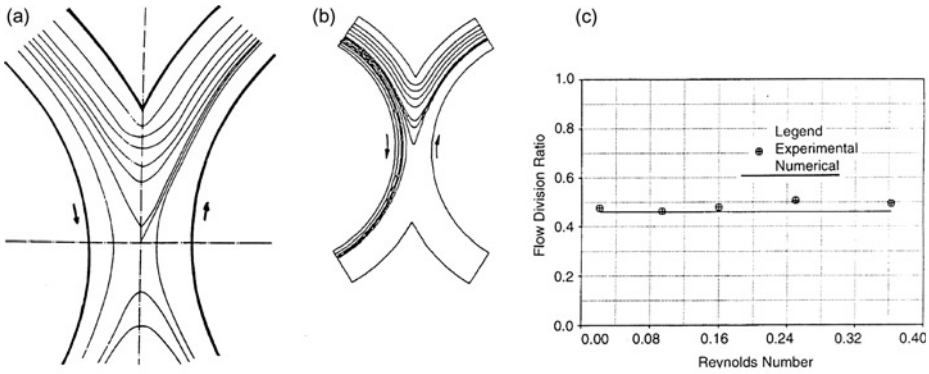

Figure 6.
Streamlines in the region between two rotating cylinders for CMC solution at 16 rpm

Notes: (a) Experimental results; (b) numerical predictions for flow entering the region over one cylinder; and (c) comparison of flow division ratio x_f obtained from experimental and numerical results

experimental and numerical results is shown, indicating good agreement at the typically small Reynolds numbers encountered in extruders. A small difference, between numerical and experimental results, arises as Reynolds numbers increase beyond 1.0, because of significant inertia effects, which were neglected in the mathematical model. For more detailed comparisons, velocity and temperature distributions have been obtained using more elaborate experimental systems and compared with the numerical results (Jaluria, 2003).

Figure 7 shows the numerical and experimental results for solidification of water in an enclosed region using the enthalpy-porosity model. The coupled conduction, or conjugate transport, in the walls of the mould is an important consideration in these problems. The effect of the imposed conditions at the outer surface of the mould on the solidification process can be obtained by solving this conjugate problem, which yields the temperature distribution in the mould as well as that in the solid and the liquid. Banaszek *et al.* (1999) carried out numerical simulations and appropriately designed experiments to demonstrate the importance of conduction in the wall, as shown in Figure 7. Velocity and temperature fields are shown, along with the ice-water interface. The streamlines indicate the effect of thermal buoyancy which causes the interface between the solid and the liquid to bend, rather than remain parallel to the vertical boundaries. The amount of material solified increases with time. The recirculation in the liquid is clearly seen. The numerical results are found to agree quite well with experimental results. Such numerical and experimental studies can be used to determine the movement of the solidification front with time and thus monitor the generation of voids and other defects in the casting. Experimental studies have been relatively few because of the complexity of the process (Viskanta, 1988). Detailed accurate experimental results are needed to critically evaluate the various models employed for simulation, as well as to provide information on the characteristics of the interface for the development of microscale models.

5. Experimentally obtained boundary conditions

In basic and practical problems that involve convective heat transfer, it is important to model the boundary conditions correctly and accurately since the accuracy and validity of the simulation are strongly affected by the transport mechanisms at the boundaries. However, the shape and location of the boundary itself are not known in

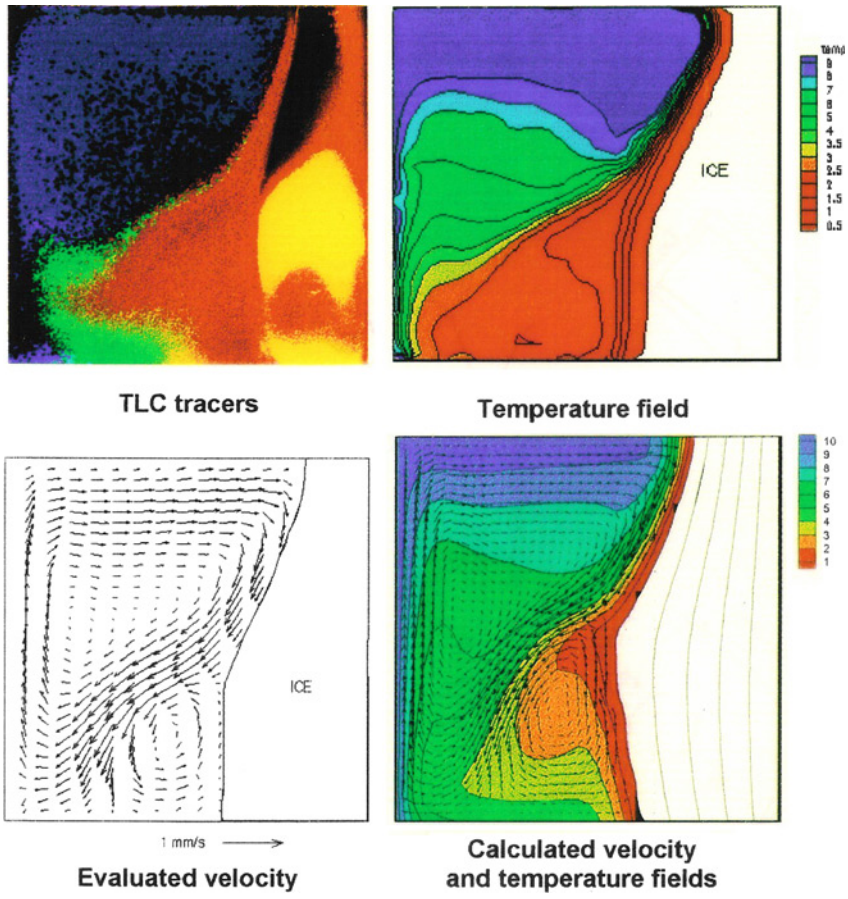

Figure 7.
Experimental and numerical results for water solidification driven by convection and conduction, with conjugate transport in the mould

some cases, such as the neck-down profile in optical fibre drawing, mentioned earlier. This is an unknown free-surface resulting from the various forces acting on the fibre, as is also the case for other free-surface flows, such as those with a meniscus. Even if the boundary is well known, the conditions at the surface may involve a coupled, much more complex problem. In such cases, the boundary conditions are obtained from a separate experiment in order to simplify the problem, or to provide inputs that are not readily available from analysis.

An example of a situation where experimentally obtained boundary conditions are frequently used to solve the problem is shown in Figure 8. The conduction problem within the rectangular two-dimensional region can easily be solved by numerical simulation if the boundary conditions are given as convective with specified ambient temperature T_f and heat transfer coefficient h, as shown in Figure 8(a). Here, h is obtained from available empirical correlations based on separate experiments on similar geometries. Such correlations are widely available and used for a fairly diverse set of problems of interest to the industry. If the heat transfer coefficient h is not given, the problem involves combined domains and a conjugate problem, as shown in Figure 8(b), which is substantially more complicated (Jaluria and Torrance, 2003). The temperature gradient at the surface in Figure 8(b) can be used to yield the heat transfer coefficient h, if needed.

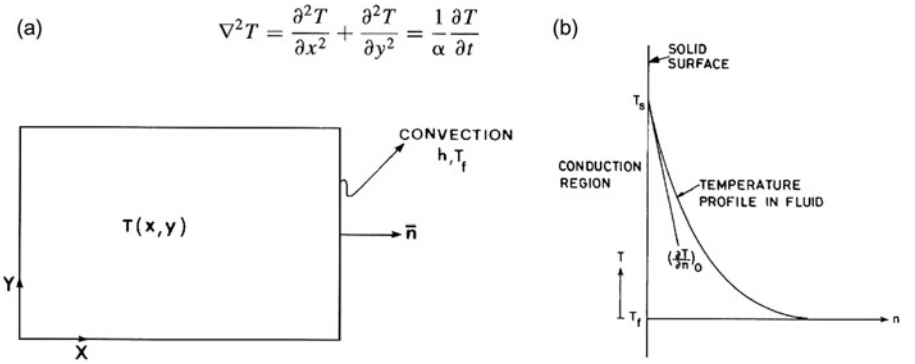

Figure 8.

Notes: (a) Conduction problem with specified convective heat transfer coefficient h at the boundaries and (b) conjugate conduction-convection problem

The nature and stability of the upper meniscus in the fibre coating process, shown in Figure 2, have been studied in detail because the moving fibre can entrap air bubbles, resulting in a deterioration of the coating. This process is strongly affected by the stability and consequent breakdown of the meniscus. The problem is very complicated because it involves a dynamic contact angle, with the fibre moving at speeds as high as 20 m/s through the air and then plunging into the liquid, with air being replaced by the liquid in the boundary layer. It is a difficult problem to model analytically or numerically. However, the shape and dimensions of the meniscus are needed to solve for the flow and convective heat transfer in the coating applicator.

Thus, this is a circumstance where experimentally obtained boundary conditions are needed for the numerical simulation to be carried out. Frequently, the shape of the meniscus is prescribed on the basis of experimental data and axisymmetric transport is assumed. The typical height of the meniscus varies from around 10 to 100 μm. The dynamic meniscus in pressurized and unpressurized fibre coating applicators has been studied experimentally by several investigators (Blyler and DiMarcello, 1980; Quere, 1999). Figure 9(a) shows the typical experimental results obtained by Abraham and Polymeropoulos (1999), Ravinutala and Polymeropoulos (2002), in terms of images of the meniscus formed with the fibre moving into a pressurized applicator. They found that the effect of the imposed pressure is to flatten the meniscus and to increase the slope of the liquid-air interface near the fibre compared to that for an unpressurized meniscus. They also studied unpressurized applicators and obtained the meniscus for a wide range of fibre speeds and fluids.

Typical numerical results obtained with a meniscus specified on the basis of these experiments are shown in Figure 9(b) from Yoo and Jaluria (2007). The computed velocity field in the applicator is shown, along with the flow near the meniscus. Even though the flow near the meniscus was found to change substantially with a change in the meniscus shape and dimensions, the flow far away was found to remain largely unaffected. A nanosecond double pulse laser source was also used to map and probe the flow field in the applicator, particularly in the vicinity of the moving 125 μm fibre, using particle image velocimetry. Good comparisons between the experimental and numerical results were obtained, lending strong support to the model.

Similarly, for optical fibre drawing in a furnace, several investigators assumed the neck-down profile on the basis of experimental data. This substantially simplified the analysis and, if experimental data are available for given ranges of the operating conditions, a specified neck-down profile can be used to reduce the complexity of the

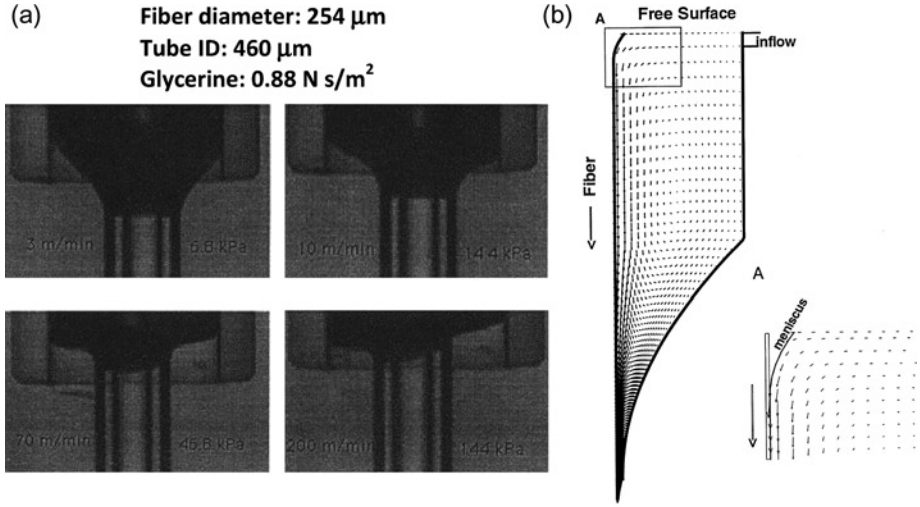

Notes: (a) Upper meniscus in optical fibre coating at different imposed pressures in the applicator and (b) numerical results with a specified upper meniscus

Figure 9.

problem and make it amenable to simulation with modest resources and effort (Roy Choudhury and Jaluria, 1998).

As another example of a practical problem where the boundary conditions are not known and experimental data are employed to define the conditions, consider the flow in a channel with isolated, protruding, heat sources, as shown in Figure 10(a). The appropriate thermal boundary conditions at the walls are not known. Conjugate conditions exist at the boundary between the cooling fluid and the walls. Boundary conditions are also needed at the openings through which the fluid enters or leaves the system. The geometry can be complicated due to the positioning of the sources and the flow configuration. The governing mass, momentum and energy conservation equations for a two-dimensional laminar natural convection flow, with constant thermophysical properties and with Boussinesq approximations, can be written in the following dimensionless form as:

$$\frac{\partial U}{\partial X} + \frac{\partial V}{\partial Y} = 0 \tag{7}$$

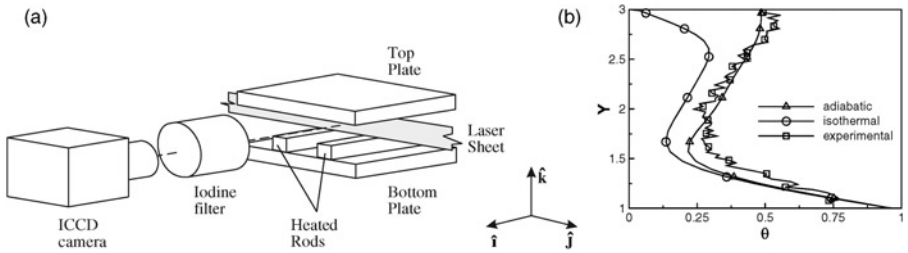

Notes: (a) Experimental system for isolated protruding heat sources in a channel with openings and (b) comparisons between numerical predictions and experiments for different boundary conditions

Figure 10.

$$\frac{\partial U}{\partial \tau}+\frac{\partial (U^2)}{\partial X}+\frac{\partial (UV)}{\partial Y}=-\frac{\partial P}{\partial X}+\Pr\left(\frac{\partial^2 U}{\partial X^2}+\frac{\partial^2 V}{\partial Y^2}\right) \tag{8}$$

$$\frac{\partial V}{\partial \tau}+\frac{\partial (UV)}{\partial X}+\frac{\partial (V^2)}{\partial Y}=-\frac{\partial P}{\partial Y}+\Pr\left(\frac{\partial^2 U}{\partial X^2}+\frac{\partial^2 V}{\partial Y^2}\right)+Gr\Pr\theta \tag{9}$$

$$\frac{\partial \theta}{\partial \tau}+\frac{\partial (U\theta)}{\partial X}+\frac{\partial (V\theta)}{\partial Y}=\frac{\partial^2 \theta}{\partial X}+\frac{\partial^2 U}{\partial Y^2} \tag{10}$$

where the dimensionless variables are defined as:

$$X=\frac{x}{h};\quad Y=\frac{y}{h};\quad U=u\frac{h}{\alpha};\quad V=v\frac{h}{\alpha};\quad \tau=t\frac{\alpha}{h^2};\quad \theta=\frac{T-T_0}{T_s-T_0};\quad P=(p-p_0)\frac{h^2}{\rho\alpha^2} \tag{11}$$

$$Gr=\frac{g\beta h^3(T_s-T_0)}{\nu^2};\quad Pr=\frac{\nu}{\alpha};\quad \beta=-\frac{1}{\rho}\left(\frac{\rho-\rho_0}{T-T_0}\right). \tag{12}$$

Figure 10(b) shows a comparison between the computed temperature distributions for the two-dimensional natural convection flow due to two sources located in the channel. The experimental study used the Filtered Rayleigh Scattering (FRS) technique to obtain the temperature profiles above the thermal sources, as shown in Figure 10(a). However, the experimental study employed a channel open on all sides and the walls were unheated. The separation between the walls was much less than the width and length of the channel. The challenge was to simulate this experiment to obtain similar trends in the predictions (Icoz and Jaluria, 2005a). The numerical results are compared with the FRS measurements in Figure 10(b) for the region above the two sources, indicating good agreement. It is found that adiabatic conditions approximate the experiment much better than isothermal conditions. However, the actual boundary conditions involve conjugate transport. Developed flow conditions were assumed at the openings and this seemed to be a satisfactory approximation. Thus, even such a simplified model is able to capture the complexity of the experiment, which can, in turn, be used to obtain the appropriate boundary conditions.

6. Solution of inverse problems with experimental inputs

There are circumstances where experiment data can be obtained over only a limited region because of access, time or other limitations. Strong constraints are thus placed on the experimental data that can be obtained through techniques such as laser and infrared diagnostics. Examples of such systems are combustors, furnaces and reactors, where only a limited access to the convective domain is available. In such cases, numerical modelling and experimentation may be used together to solve an inverse problem in order to define and quantify the boundary conditions and then proceed to the numerical simulation of the complete problem. Thus, detailed quantitative information on the flow, temperature and other quantities, which is needed in order to

optimize the system as well as to control the process, is obtained through the numerical solution of an inverse problem with selective experimental inputs.

An important example of such limited access is the optical fibre drawing furnace, shown in Figure 11. This high-temperature furnace typically has an infrared sensor to monitor the temperature of the heating element at only one location and to use its output for control (Issa *et al.*, 1996; Paek, 1999). The boundary conditions, particularly the thermal conditions, are not very well known. The temperature distribution at the wall is the result of the heat transfer mechanisms, particularly radiation, operating in the furnace and is not a known input to the numerical model. The temperature distribution affects the material properties, as well as the transport processes. It is thus a critical variable in the calculation of the glass flow, which then yields the characteristics of the fibre. The energy input to the heating element is known, along with the geometry and material characteristics. But the resulting wall temperature distribution is not easily obtained and is thus largely an unknown parameter. In such cases, the limited data that can be obtained by experiment is used in conjunction with numerical modelling to solve an inverse problem to determine the wall temperature distribution.

Issa *et al.* (1996) obtained temperature measurements at the centreline of a rod placed at the axis of the furnace. An experimental procedure involving mounting rods of different materials and diameters axially within the furnace cavity was employed for this purpose. Each rod was instrumented with thermocouples inserted through an axial hole along the centreline. The temperature measurements were used along with a numerical model for the flow and heat transfer in the furnace in order to obtain the furnace wall temperature profile. This is an inverse problem since the centreline temperature in the rod is known, whereas the furnace thermal conditions are not known. Then, they solved this inverse problem numerically to determine the wall temperature distribution that yielded the temperature measurements obtained in the graphite rod. An optimization technique was used to ensure that the result of the inverse calculation was essentially unique. The results obtained using graphite rods suggest that the furnace temperature is not significantly affected by rod size, over the desired range of 0.5-2.0 cm. A study of the flow and thermal transport associated with the draw furnace require accurate knowledge of the furnace wall temperature distribution. Figure 11(b) shows the computed temperature distribution along the graphite heating element. The dashed lines represent the water-cooled portion of the

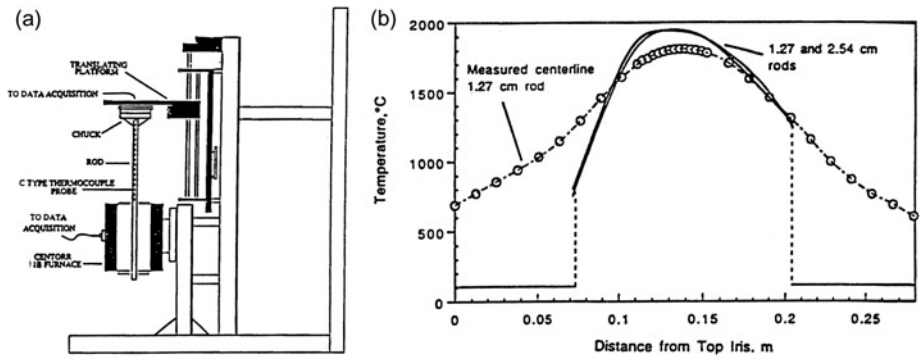

Notes: (a) Experimental system to measure the centreline temperature of graphite rods placed at the axis of the fibre draw furnace and (b) measured and calculated centreline temperatures in the graphite rods, along with the predicted furnace wall temperature distribution

Figure 11.

furnace wall. The convergence of the optimization method used for deriving the heating element temperature distribution is demonstrated by the agreement between the predicted and measured rod temperatures. The computed maximum element temperatures were in good agreement with the furnace sensor temperature at the hot zone centreline, lending support to the model for the transport processes in the furnace. Similar results were obtained for the other furnace temperatures and for other materials, including silica glass.

This approach was used for another practical system, the single-screw polymer extruder, shown in Figure 12. The system consists of a rotating screw and a heated/cooled barrel, as described earlier. The temperature at the inner surface of the barrel is critical in the computation of the flow, heat transfer, pressure and material changes in the extruder. However, the system involves a complicated, multi-region, conjugate problem, without well-known conditions at the outer surface. Access to the barrel wall is limited in practical systems because of the expense and complex geometry. Therefore, the approach outlined above may be used effectively. Limited experimental temperature data at the barrel wall and at the exit of the extruder may be used along with numerical simulation of the flow in the extruder to solve an inverse problem to determine the barrel temperature distribution accurately and uniquely. This temperature distribution is then taken as an input to the computational model to calculate the conditions within the extruder, as shown in

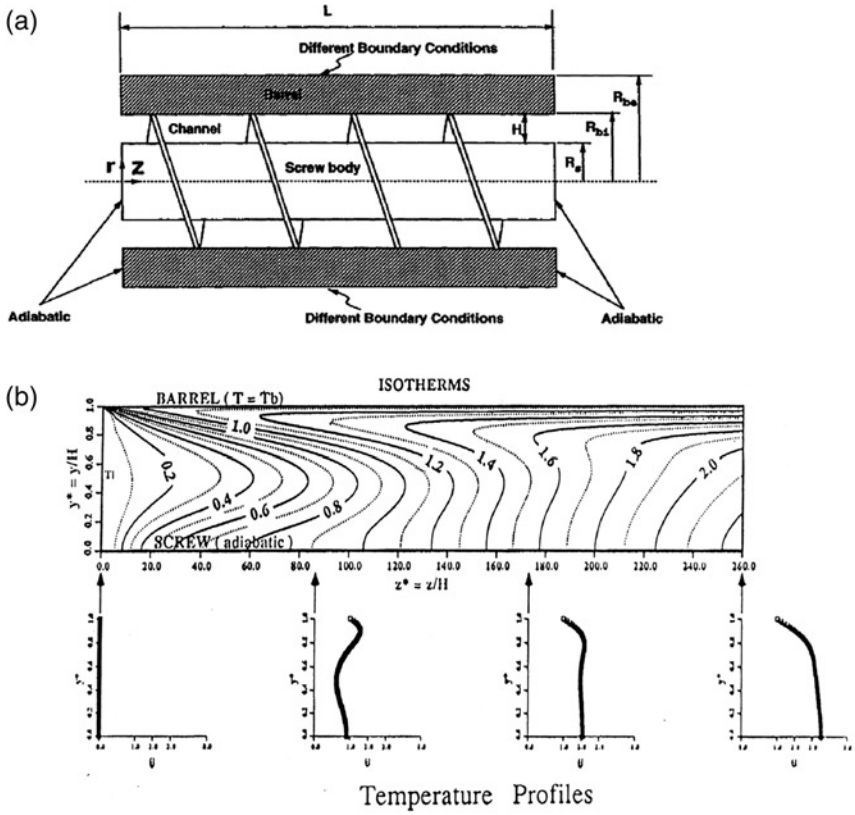

Figure 12.

Notes: (a) Single-screw extruder system, showing conjugate transport in the barrel and (b) calculated temperature field in the extruder channel

Figure 12(b) in terms of the calculated isotherms. Substantial work has been done on this problem as well (Jaluria, 1996) and only a brief description is given here.

The preceding consideration can be further employed to develop dynamic data-driven applications systems (DDDAS), which is an innovative approach to engineering research based upon the synergistic interaction between experiment and simulation. There are two different implementations of DDDAS: Open Loop and Closed Loop. In Open Loop, experimental data is streamed into the simulation (or vice versa) to achieve greater accuracy, detail and/or robustness. An example is real-time streaming of meteorological measurements into weather simulations. In Closed Loop, experiment and simulation interact in an iterative manner, i.e. the experiment guides the simulation and the simulation in turn guides the experiment (Darema, 2004; Mandel *et al.*, 2004). The DDDAS approach has been widely applied in engineering and science. Knight *et al.* (2002) and Zhao *et al.* (2007) applied the DDDAS concept to engineering design with the development of the data-driven design optimization methodology. This approach synergizes experiment and simulation in a manner, which exploits the advantages, and recognizes the limitations, of each approach, as discussed in the following section. This effort focuses on the assessment of fluid-thermal systems that are characterized by two major limitations, namely:

(1) The experimental measurements are limited to diagnostics in restricted regions of the flow, as seen above.

(2) There is incomplete a priori specification of the boundary conditions for the flow simulation, as also discussed earlier.

The approach is founded on the Closed Loop DDDAS concept wherein the experiment directs the simulation and vice versa. The method approximates the unknown boundary conditions for the simulations by minimizing the error in the prediction of the measured data and identifies needed subsequent experimental measurements to reduce the error. The result is a complete assessment of the fluid-thermal system. Neither the experiments alone, nor any simulation based on the a priori boundary conditions, can provide a complete assessment of the fluid-thermal system. However, the synergism of experiment and simulation based upon the DDDAS concept yields a complete assessment of the fluid-thermal system (Knight *et al.*, 2006; Ma *et al.*, 2006).

To further discuss this methodology, let us consider a jet in cross-flow, as shown in Figure 13(a). This flow is important in the evaluation of environmental effects of thermal and material discharges into the environment. If limited data taken downstream can be used to determine the location and conditions at the inlet, it would allow the determination of polluting source as well as the impact on the environment. In many cases, information on the source is not known, though information downstream can be obtained. This circumstance can be simplified in terms of a rectangular jet injected perpendicular to an incompressible air flow, as shown in Figure 13(b). The inflow is an equilibrium laminar boundary layer in air defined by the specified free stream conditions, velocity U_∞ and temperature T_∞. The jet is defined by the jet average velocity U_j and temperature T_j. The computational domain is shown. For the simulations, the free stream conditions are assumed to be known. By analogy to the optical fibre drawing furnace, the jet average velocity U_j and temperature T_j are assumed unknown. The objective is then the determination of the jet average velocity U_j and temperature T_j based upon a Closed Loop DDDAS methodology.

The experiments were performed in a low-speed wind tunnel, with a test section of 0.7×0.7 m in cross-section and a length of 2 m. The maximum velocity in the test section

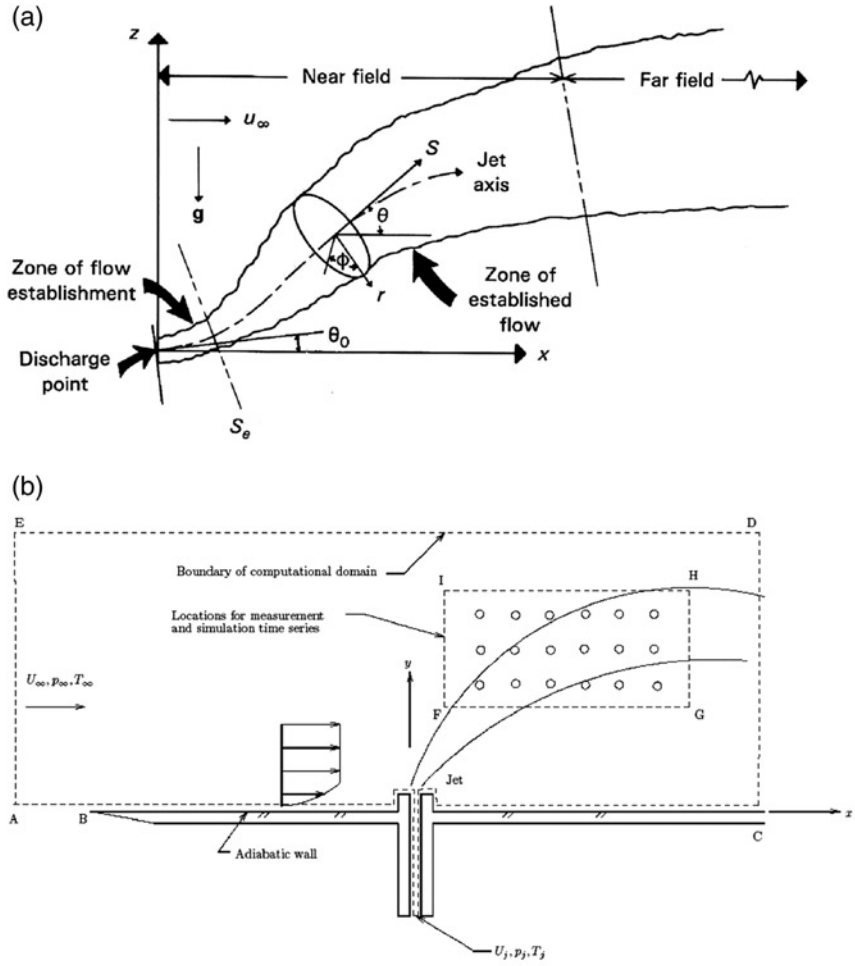

Figure 13.

Notes: (a) Buoyant jet due to thermal or material discharge in a crossflow and (b) arrangement to predict discharge conditions from downstream measurements

is 30 m/s and is measured using a traversing pitot tube and wall pressure taps. The wind tunnel velocity is controlled using LabView. A two-dimensional slot jet protrudes from a flat plate with the jet centreline at a distance of 188 mm from the leading edge of the plate. The flat plate has a sharp leading edge and is raised 50 mm above the wind tunnel floor to avoid the tunnel floor boundary layer. The jet slot width is 3.2 mm and the spanwise depth is 545 mm. The jet fences protrude 8.8 mm above the flat plate and each fence is 6.4 mm wide in the x-direction. A diode laser system is used to measure the time-varying absorbance across the flow field in the spanwise direction at selected locations. A 761 nm Vertical Cavity Surface Emitting Laser is placed in a temperature controlled housing (ILX Lightwave 4412). The output wavelength is modulated by the injection current (ILX Lightwave Diode Laser Controller, LDC-3714B). Since the flow field is unsteady (as shown by the CFD simulations) at a fundamental frequency of approximately 20 Hz with higher order harmonics, the diode laser system was scanned at 400 Hz. The experimental

temperature was measured using both the laser absorbance method and by a thermocouple. Additional details are presented by Ma *et al.* (2006).

A validation study was performed to assess the accuracy of the simulations by comparison with experiment. The difference between the computed and measured mean temperature was found to vary from 0.2 to 10.5 per cent. The variation between the laser and thermocouple measurements ranges from 2.4 to 10.8 per cent. It is noted, however, that the thermocouple measures the temperature at a single point, whereas the laser absorbance is an integrated instantaneous measurement of the temperature over the span of the wind tunnel. Small instantaneous variations of the flow field in the spanwise direction will therefore cause a difference between the laser absorbance and thermocouple measurements. Moreover, the simulations are time-accurate two-dimensional, and therefore do not take into account possible small three-dimensional effects. We may conservatively conclude that the simulation is capable of prediction of the experimental mean temperature within 10 K.

The Closed Loop DDDAS methodology was applied to determine the unknown jet velocity U_j and jet temperature difference $\Delta T_j = T_j - T_\infty$, as shown in Figure 14. First, six locations were selected and the predictions from the simulations were used to build the Response Surface Model. Next, the experiment was performed with the jet velocity U_j and temperature T_j selected by the experimentalists but not communicated to the person performing the Closed Loop DDDAS Method. The experimental mean temperature at the six selected locations was provided to the Response Surface Model. The predictions of U_j and ΔT_j based upon the Response Surface Model were found to be 7 ± 1 m/s and 117 ± 3 K. The uncertainty of ± 1 m/s in the predicted value of U_j is attributable to the uncertainty in the experimental U_∞ (i.e. $U_\infty = 4.0 \pm 0.5$ m/s). The uncertainty in the predicted value of ΔT_j is the standard deviation of the best fit to the Response Surface Model over the range of possible number of locations used to minimize the mean square error E. In Step No. 2, the Response Surface Models were used to select four additional locations. The second experiment was performed and the mean temperature at the four additional locations was provided to the Response Surface Model. The predictions of U_j and ΔT_j based upon the Response Surface Model were 7 ± 1 m/s and 129 ± 9 K. Thereafter, the experimental values of U_j and ΔT_j were announced. The experimental values were $U_j = 7.97$ m/s and $\Delta T_j = 107 \pm 5°$ K. Thus, the Closed Loop DDDAS methodology predicted the jet velocity U_j within the experimental uncertainty associated with U_∞ but over predicted ΔT_j by 9 per cent in

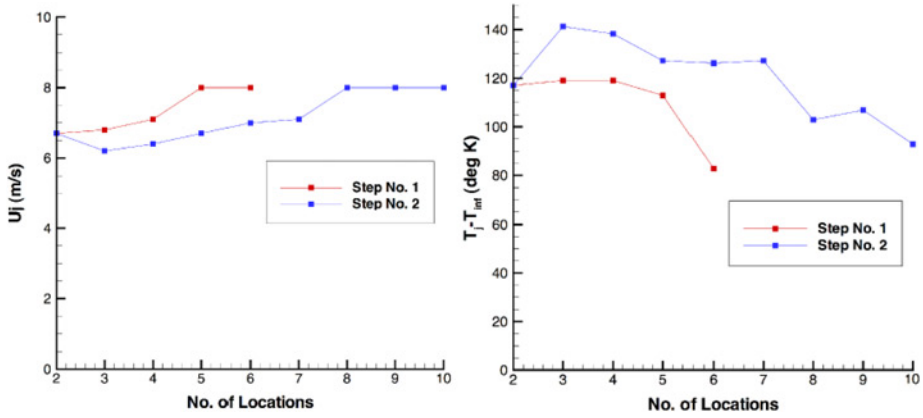

Figure 14.
Results from applying the DDDAS methodology to the flow circumstance of Figure 13(b)

the first step and by 21 per cent in the second step. The over prediction of 9 per cent in the first step is comparable to the validated accuracy of the two-dimensional simulations compared to the experiment.

Thus, the DDDAS method can be employed for assessing fluid-thermal systems wherein the complete boundary conditions are not known a priori. A simple example of the temperature and velocity for a jet in cross flow is given here, but the approach can be extended to more complicated problems. Current effort is being directed at such problems, for example, the determination of the location and energy input of a fire in an extensive or enclosed region. By measuring temperatures at the door or at a wall, the methodology can be used to predict the location and conditions of the source, thus impacting on fire safety, prediction and control.

7. Concurrent simulation and experimentation

In the solution of practical convection problems, it is often found that numerical simulation is particularly suitable over a certain domain, whereas experimentation is more appropriate and accurate over other domains. Then, the two could be used concurrently to obtain a more efficient approach to solving the problem. This is particularly valuable in system design and optimization.

Conventional engineering design and optimization are based on sequential use of computer simulation and experiment, with the experiments generally being used for validation or for providing selective inputs, as discussed earlier. However, the conventional methods fail to use the advantages of using experiment and simulation concurrently in real time. Numerical simulation can easily accommodate changes in geometry, dimensions and material, whereas experiments can more conveniently study variations in the operating conditions such as flow rate, imposed pressure and heat input. Also, laminar and stable flows can be simulated conveniently and accurately, whereas transitional and turbulent flows are often more accurately investigated experimentally. By using concurrent numerical simulation and experimentation, the entire domain of interest can be studied for system design and optimization efficiently and accurately. This is the main motivation for this approach.

Consider the simple physical system shown in Figure 15, consisting of multiple isolated heat sources, which approximate electronic components, located in a horizontal channel in a two-dimensional configuration (Incropera, 1988; Sathe and Sammakia, 1998). A square vortex promoter of side h_p is also shown in the figure to induce oscillatory flow and thus enhance heat transfer. The height and width of the

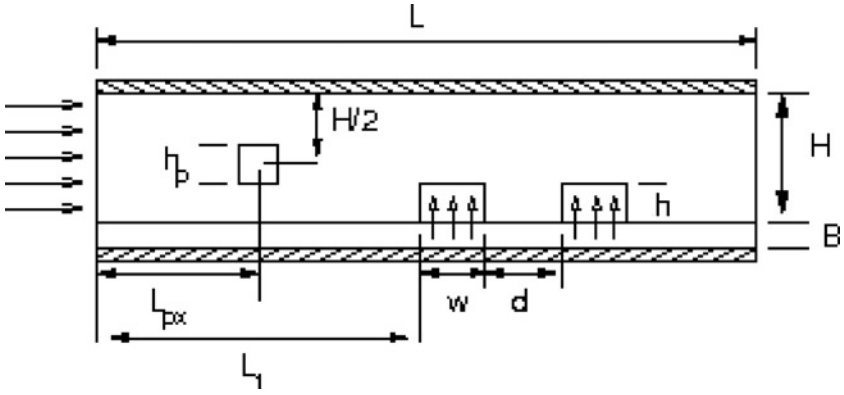

Figure 15.
Two heating elements, simulating electronic components, in a channel with a uniform forced flow at the inlet and a vortex promoter

sources are h and w, respectively. The heat sources are separated by distance d. The thickness of the bottom plate is B. The problem involves removing the energy dissipated by these components by the flow of air or a liquid. The flow conditions are defined by Re and Gr, both being based on the channel height. The fluid is represented by its properties, particularly the Prandtl number Pr. Variables include the inlet fluid velocity, heat input to the components, channel dimensions, coolant, location and orientation of the heat sources. Typical design objectives are maximizing the heat removal rate from the components and minimizing the pressure drop. The temperature and pressure drop have to be kept below some allowable limits, T_{wo}, ΔP_o. Numerical and experimental methods are to be used concurrently to study a wide range of design variables and operating conditions. The overall inputs required for the design and optimization of the system are obtained using numerical simulation for low flow rates and heat inputs and experimental systems for larger values. The switch from simulation to experiment is determined based on the critical values of Re and Gr values for transition to turbulence (Icoz and Jaluria, 2005b). Two experimental setups have been used in this study, one for air and the other for liquid cooling. The experiments for air are performed for Re = 1,000-5,200. A similar arrangement is used for water. The liquid cooling experiments are performed to study the free and mixed convective heat transfer characteristics of two flush mounted discrete heat sources. The Reynolds number based on the channel height is varied in the range from 2,800 to 5,800.

Numerical simulation can be used very satisfactorily for low Re and Gr. The governing non-dimensional differential equations for laminar mixed convection flow, with constant thermophysical properties can be written in the following form:

$$\nabla \cdot \vec{V} = 0 \tag{13}$$

$$\frac{\partial \vec{V}}{\partial \tau} + \vec{V} \cdot \nabla \vec{V} = -\nabla P + \frac{1}{\mathrm{Re}} \nabla^2 \vec{V} - \frac{Gr}{\mathrm{Re}^2} \theta \cdot \vec{g} \tag{14}$$

$$\frac{\partial \theta}{\partial \tau} + \vec{V} \cdot \nabla \theta = \frac{1}{\mathrm{RePr}} \nabla^2 \theta. \tag{15}$$

Conduction equation within the bottom plate (substrate):

$$\frac{\partial \theta}{\partial \tau} = \frac{1}{\mathrm{RePr}} \nabla^2 \theta \tag{16}$$

where the dimensionless variables are defined as:

$$X = \frac{x}{H}; \quad Y = \frac{y}{H}; \quad U = \frac{u}{U_m}; \quad V \frac{v}{U_m}; \tag{17}$$

$$\tau = t \frac{U_m}{H}; \quad \theta = \frac{T - T_0}{T_s - T_0}; \quad P = \frac{p - p_0}{\rho U_m^2}; \tag{18}$$

$$Gr = \frac{g\beta \cdot h^3 (T_s - T_0)}{v^2}; \quad \mathrm{Pr} = \frac{v}{\alpha}; \quad \beta = -\frac{1}{\rho} \left(\frac{\rho - \rho_0}{T - T_0} \right). \tag{19}$$

The boundary conditions implemented here involve fully developed axial and zero

vertical velocity at the inlet at ambient temperature, fully developed flow conditions at the exit, no-slip conditions and adiabatic surface assumption at top and bottom walls.

To validate the code, the computed results are compared to the results obtained by Kim *et al.* (1992, 1998) for forced convection in a channel problem with Re = 750. The local Nusselt number along the first heat source surface was plotted and two results showed very good agreement, validating the present results (Icoz *et al.*, 2006).

The temperature and velocity distributions, the heat removal rates and pressure drop are then calculated for laminar flows, as well as the beginning of oscillatory flow. Experiments are used for translational and turbulent flows. The first part of the simulation results deals with the determination of the critical flow conditions up to which numerical simulation can be used satisfactorily. The Gr value, which is set at 7.2×10^5, is constant for all computations because the heat sources are treated as isothermal elements, at a temperature of 60 °C above ambient, and the channel height, which is kept constant throughout the study, is chosen as the characteristic length for non-dimensional parameters, such as Re and Gr. The critical Re value is determined by observing the transient change in Nu values as a function of time for different Re values. The transient results reveal that the onset of unsteady flow starts at around Re = 1,500. Similarly, other geometries and conditions were investigated.

The basic approach outlined here was used for liquid cooling and also for enhanced heat transfer with the use of a vortex promoter in the channel (Icoz and Jaluria, 2006). Typical results are shown in Figure 16. The increase in the heat transfer due to the presence of a passive vortex promoter in the channel flow was determined and concurrent simulation and experimentation was used to obtain the heat transfer and pressure results, as shown in Figure 17. This figure shows the heat transfer rates Q_1

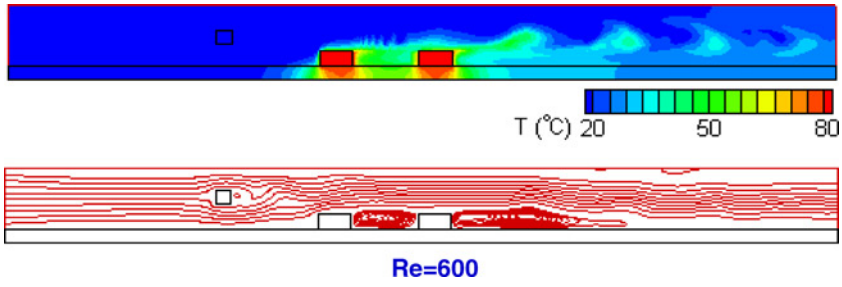

Figure 16.
Flow and thermal fields due to a vortex promoter and isolated thermal sources in a channel with forced flow

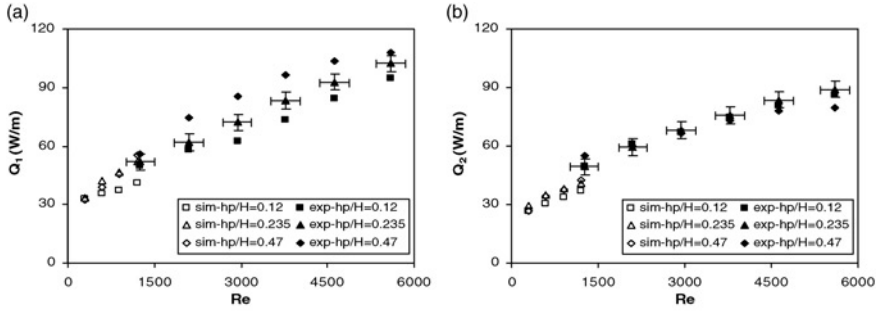

Figure 17.
Computed and measured (shown with uncertainty) heat transfer rates as functions of Re

Notes: (a) First heat source and (b) second heat source, for flow in a channel with a vortex promoter

and Q_2 for the two sources (Q_1 being for the source closer to the inlet) obtained from numerical simulation at low Re and from experiment at large Re. There is fairly good agreement between the two in the overlapping region, though there is uncertainty in the experimental data, as indicated here. These results were used to generate the response curves, from which optimal conditions were obtained. The shape of the promoter was also taken as a parameter, along with the channel height and source geometry. The operating conditions were also varied. Other optimization strategies were also used, but the input data needed for all these were obtained by concurrent simulation and experimentation. For additional results and further details, see Knight *et al.* (2002), Icoz and Jaluria (2006), Zhao *et al.* (2007).

Similar results were obtained for the sources in the channel without the promoter, as shown in Figure 18, which included results on Q_1 and on Δp. There is greater uncertainty in the experimental data for the pressure, as compared to that for the heat transfer rate. But there is reasonable agreement between the experimental and numerical results. Also, the two approaches are used concurrently to cover the entire domain. Similarly, parameters like geometry, dimensions and materials were varied in the search for the optimal design. Again, response surfaces were obtained and optimal conditions were determined. Figure 19 shows the variation of a composite objective

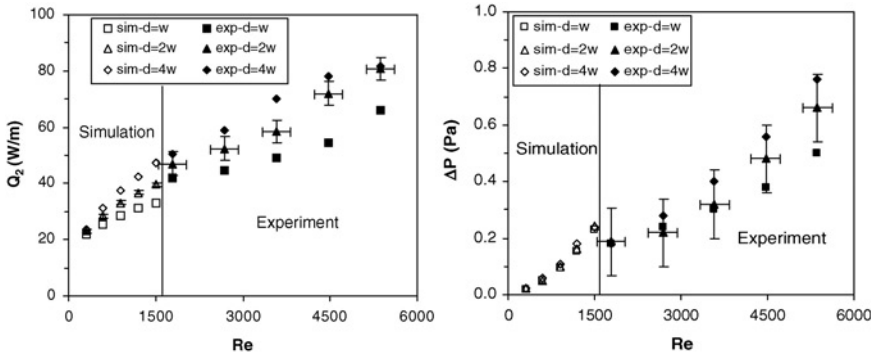

Figure 18.
Computed and measured heat transfer rate from the first heat source and pressure drop as functions of Re and geometry, for flow in a channel without a vortex promoter

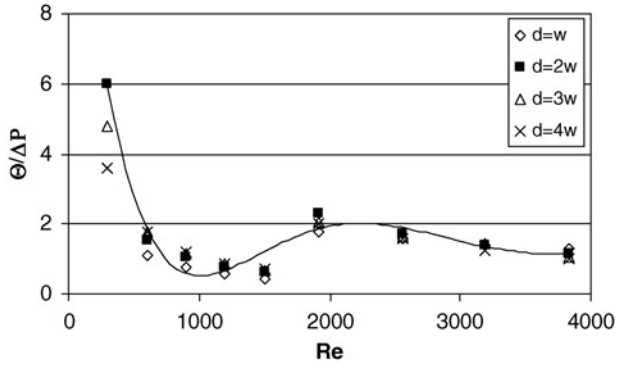

Figure 19.
Optimization of the system with two isolated heat sources in a channel with forced flow, using a composite objective function

function, which includes both the source temperature and the pressure drop, so that the minimum in the objective function is sought for the optimum.

This is really a multi-objective function problem and has to be handled by considering the two objective functions separately. But this simple approach of combining the objectives into a single function simplifies the problem. The weighted sums method (Deb, 2002), may also be employed in the form of:

$$F = \sum W_i F_i(x_1, x_2, x_3) \tag{20}$$

where W_i ($\in [0, 1]$) is the weight of the i-th objective function, and $\sum W_i = 1$. The global optimal points and the value of the objective function for various weights were obtained. It was found that as the weight of the pressure drop is decreased to $W_1/2$ the optimal point is at the maximum values of the design variables. This is because the maximum heat transfer rates are obtained at the same point, and making ΔP less important by setting its weight a smaller value shifts the optimal point to the maximum values of the design variables. However, as the importance of ΔP increases, the optimal values of the design variables get smaller. When W_3 is set $2 \times W_1$ and $3 \times W_1$ the optimal value of Re drops to 2,855-1,450, respectively. The optimal heat source height is found to be either $h/H = 0.35$ or 0.15 depending on the relative importance of the individual objective functions. If maximizing the heat transfer rates is the primary design objective, the optimal h/H is found to be 0.35. If minimizing the pressure drop is more important than the heat transfer rate, h/H is found to be 0.15. The optimal values of Re and d for a given of h/H, when the performance of individual heat sources is of interest, were also obtained. The results reveal that the optimal Re value does not change significantly with h/H. For the objective function of maximizing $\bar{Q}_1 - \Delta\bar{P}$, Re falls in the range of 3,000-3,400, and for the objective function of $\bar{Q}_2 - \Delta\bar{P}$, it varies between 1,900 and 2,200. Similar results arise for liquid cooling. A comparison of cooling capabilities of natural convection of air and de-ionized water was performed. Results show that the heat transfer coefficient for water is around 19 times greater than that for air. The maximum heat transfer coefficient attained when $d = 3.5$ w is found to be 18 W/m^{2K} for air and 350 W/m^{2K} for water.

Therefore, it is shown that numerical simulation and experimentation can be used concurrently to yield an efficient approach to cover the entire operational domain and thus provide inputs needed for understanding the operation of the system, as well as for design and optimization. Though only a few simple circumstances are discussed here, the approach was used for more complicated circumstances such as the design of extruder systems, particularly dies, supersonic aircraft inlet and the system for polymer injection treatment of osteoporosis in human orthopedic systems.

8. Conclusions

Experimentation is needed in a wide range of basic and applied convective heat transfer problems in order to provide the inputs needed for accurately defining the boundary conditions, simplifying the modelling and obtaining results over regions where simulation is inaccurate, inconvenient or inefficient. In addition, experimental data are needed for material properties and for the validation of the models used. The accuracy of the numerical results depends strongly on the material properties. This paper presents various circumstances where the numerical simulation may be efficiently combined with experimentation, and indeed driven by experimental data, to

obtain accurate, valid and realistic numerical predictions. Several examples of such problems are given and the difficulties with specifying the boundary conditions as well as with simulating the entire domain for design and optimization are outlined. Approaches for using experimental data-driven simulation in such cases are discussed and results are presented for some simple and complex problems. It is shown that such approaches are critical to an accurate numerical simulation in many cases of practical interest. The basic methodology is presented and the present status as well as the needed future work is discussed. The review paper thus focuses on the role played by experimentation in an accurate numerical simulation of thermal processes and systems.

References

Abraham, A. and Polymeropoulos, C.E. (1999), "Dynamic menisci on moving fibers", *The Proceedings of the 48th International Wire* and *Cable Symposium*, *Atlantic City, NJ*.

Banaszek, J., Jaluria, Y., Kowalewski, T.A. and Rebow, M. (1999), "Semi-implicit FEM analysis of natural convection in freezing water", *Numerical Heat Transfer*, Vol. 36, pp. 449-72.

Blyler, L.L. and DiMarcello, F.V. (1980), "Fiber drawing, coating and jacketing", *Proceedings of the IEEE*, Vol. 68, pp. 1194-8.

Darema, F. (2004), "Dynamic data driven application systems: a new paradigm for application simulations and measurements", *Fourth International Conference on Computational Science*, Springer-Verlag, Berlin, pp. 662-9.

Deb, K. (2002), *Multi-objective Optimization Using Evolutionary Algorithms*, John Wiley & Sons, New York, NY.

De Vahl Davis, G. and Leonardi, E. (Eds) (2001), *Advances in Computational Heat Transfer II*, Begell House Pub., New York, NY.

Icoz, T. and Jaluria, Y. (2005a), "Numerical simulation of boundary conditions and the onset of instability in natural convection due to protruding thermal sources in an open rectangular channel", *Numerical Heat Transfer*, Vol. 48, pp. 831-47.

Icoz, T. and Jaluria, Y. (2005b), "Design of cooling systems for electronic equipment using both experimental and numerical inputs", *ASME Journal of Electronic Packaging*, Vol. 126, pp. 465-71.

Icoz, T. and Jaluria, Y. (2006), "Design optimization of size and geometry of vortex promoter in a two-dimensional channel", *ASME Journal of Heat Transfer*, Vol. 128, pp. 1081-92.

Icoz, T., Verma, N. and Jaluria, Y. (2006), "Design of air and liquid cooling systems for electronic components using concurrent simulation and experiment", *ASME Journal of Electronic Packaging*, Vol. 128, pp. 466-78.

Incropera, F.P. (1988), "Convection heat transfer in electronic equipment cooling", *ASME Journal of Heat Transfer*, Vol. 110, pp. 1097-111.

Issa, J., Yin, Z., Polymeropoulos, C.E. and Jaluria, Y. (1996), "Temperature distribution in an optical fiber draw tower furnace", *Journal of Materials Processing and Manufacturing Science*, Vol. 4, pp. 221-32.

Jaluria, Y. (1996), "Heat and mass transfer in the extrusion of non-Newtonian materials", *Advances in Heat Transfer Series*, Vol. 28, pp. 145-230.

Jaluria, Y. (2003), "Thermal processing of materials: from basic research to engineering", *ASME Journal of Heat Transfer*, Vol. 125, pp. 957-79.

Jaluria, Y. (2008), *Design and Optimization of Thermal Systems*, 2nd ed., CRC Press, Boca Raton, FL.

Jaluria, Y. and Torrance, K.E. (2003), *Computational Heat Transfer*, 2nd ed., Taylor & Francis, New York, NY.

Karwe, M.V. and Jaluria, Y. (1990), "Numerical simulation of fluid flow and heat transfer in a single-screw extruder for non-newtonian fluids", *Numerical Heat Transfer*, Vol. 17, pp. 167-90.

Kim, S.Y., Kang, B.H. and Jaluria, Y. (1998), "Thermal interaction between isolated heated electronic components in pulsating channel flow", *Numerical Heat Transfer, Part A*, Vol. 34, pp. 1-21.

Kim, S.Y., Sung, H.J. and Hyun, J.M. (1992), "Mixed convection from multiple-layered boards with cross-streamwise periodic boundary conditions", *International Journal of Heat and Mass Transfer*, Vol. 35, pp. 2941-52.

Knight, D., Rossman, T. and Jaluria, Y. (2006), "Evaluation of fluid-thermal systems by dynamic data driven application systems", *International Conference on Computational Science (ICCS06)*, Reading, MA.

Knight, D., Elliott, G., Jaluria, Y., Langrana, N. and Rasheed, K. (2002), "Automated optimal design using concurrent integrated experiment and simulation", AIAA Paper No. 2002-5636, AIAA, Reston, VA.

Ma, Q., Luo, Y., Rossman, T., Knight, D. and Jaluria, Y. (2006), "Measurements for DDDAS: flow field reconstruction using experimental and numerical data", *AIAA Aerodynamic Measurement Technology and Ground Testing Conference, AIAA, Reston, VA*.

Mandel, J., Chen, M., Franca, L., Johns, C., Pulhalskii, A., Coen, J., Douglas, C., Kremens, R., Vodacek, A. and Zhao, W. (2004), "A note on dynamic data driven wildfire modeling", *Fourth International Conference on Computational Science*, Springer-Verlag, Berlin, pp. 725-31.

Moore, F.K. and Jaluria, Y. (1972), "Thermal effects of power plants on lakes", *ASME Journal of Heat Transfer*, Vol. 94, pp. 163-68.

Paek, U.C. (1999), "Free drawing and polymer coating of silica glass optical fibers", *ASME Journal of Heat transfer*, Vol. 121, pp. 774-88.

Patankar, S.V. (1980), *Numerical Heat Transfer and Fluid Flow*, Taylor and Francis, New York, NY.

Quere, D. (1999), "Fluid coating on a fiber", *Annual Review of Fluid Mechanics*, Vol. 31, pp. 347-84.

Ravinutala, S. and Polymeropoulos, C.E. (2002), "Entrance meniscus in a pressurized optical fiber coating applicator", *International Journal of Experimental Heat Transfer and Fluid Mechanics*, Vol. 26, pp. 573-80.

Roache, P.J. (1998), *Verification and Validation in Computational Science and Engineering*, Hermosa Publishers, Albuquerque, NM.

Roy Choudhury, S. and Jaluria, Y. (1998), "Practical aspects in the drawing of an optical fiber", *Journal of Materials Research*, Vol. 13, pp. 483-93.

Sathe, S. and Sammakia, B. (1998), "A review of recent developments in some practical aspects of air-cooled electronic packages", *ASME Journal of Heat Transfer*, Vol. 120, pp. 830-9.

Sastrohartono, T., Esseghir, M., Kwon, T.H. and Sernas, V. (1990), "Numerical and experimental studies of the flow in the nip region of a partially intermeshing co-rotating twin screw extruder", *Polymer Engineering and Science*, Vol. 30, pp. 1382-98.

Tadmor, Z. and Gogos, C. (1979), *Principles of Polymer Processing*, Wiley, New York, NY.

Viskanta, R. (1988), "Heat transfer during melting and solidification of metals", *ASME Journal of Heat Transfer*, Vol. 110, pp. 1205-19.

Yin, Z. and Jaluria, Y. (1997), "Zonal method to model radiative transport in an optical fiber drawing furnace", *ASME Journal of Heat Transfer*, Vol. 119, pp. 597-603.

Yoo, S.Y. and Jaluria, Y. (2007), "Fluid flow and heat transfer in an optical fiber coating process", *International Journal of Heat Mass Transfer*, Vol. 50, pp. 1176-85.

Zhao, H., Icoz, T., Jaluria, Y. and Knight, D. (2007), "Application of data driven design optimization methodology to a multi-objective design optimization problem", *Journal of Engineering Design*, Vol. 18, pp. 343-59.

Corresponding author
Yogesh Jaluria can be contacted at: jaluria@jove.rutgers.edu

To purchase reprints of this article please e-mail: **reprints@emeraldinsight.com**
Or visit our web site for further details: **www.emeraldinsight.com/reprints**